

*Krzysztof Rusin*

**Silesian University of Technology**

Konarskiego 18, 44-100 Gliwice, Poland, [krzysztof.rusin@polsl.pl](mailto:krzysztof.rusin@polsl.pl)

## THE INFLUENCE OF OUTLET SYSTEM GEOMETRY ON TESLA TURBINE WORKING PARAMETERS

### Abstract

The paper presents an analysis of the influence of Tesla turbine outlet system geometry on parameter distribution and power. Simulations were carried out with the aid of Ansys products: DesignModeler, Meshing and CFX 17.0. The model geometry was based on the dimensions of existing turbine. Three different types of outlet system were investigated. A mesh independence study was carried out in order to obtain results which were unaffected by discretization method. Computations were performed using experimental data. The flow phenomena occurring inside the turbine are described in addition to the differences caused by outlet system geometry. Numerical results were confronted with experimental analysis.

### Key words

Tesla turbine, CFD, bladeless turbine

### Introduction

Tesla turbine, also known as the bladeless turbine, was manufactured for the first time in 1906 by Nikola Tesla and was patented in 1913 [1]. Due to lack of funds and materials able to withstand tensile stresses, Tesla was forced to abandon investigation into this turbine type. Developments in materials technology and unique advantages have resulted in a renewed interest in bladeless turbine. Many experimental analysis have been performed, which have contributed to broaden the knowledge of flow in the Tesla turbine. Lemma et al. [2] carried out experimental analysis of the Tesla turbine with 50 mm diameter rotor with the air as working medium. The highest obtained efficiency was 23.1%. Hoya and Guha [3] constructed turbine with rotor diameter of 92 mm. They obtained the highest efficiency of 25% and power of 140 W.

Tesla turbine has many advantages [4], including among others: a simple geometry which significantly decreases manufacturing cost, resistance to erosion and high flexibility in choice of working medium. These advantages allow for the opportunity to use bladeless turbines in ORC installations or installations powered by renewable energy sources. Lampart and Jędrzejewski [5] performed numerical analysis of Tesla turbine using a low boiling medium. The results proved, that isentropic efficiency could reach 50%. Ho-Yan [6] performed analytical investigation of Tesla turbine for pico hydro applications. Carey [7] analysed use of Tesla turbine for small scale Rankine system. He derived dimensionless parameters and determined their values, which could provide turbine isentropic efficiency within range of 80-90%. Sengupta and Guha [8] performed computational and experimental analysis concerning flow of a nanofluid in Tesla turbine. They proved that use of nanofluids can increase generated power without any major drop in efficiency.

The principle of operation of the turbine is based on the phenomena of adhesion and viscosity. The working fluid adheres to the disc's surface because the adhesive forces between fluid particles and disc particles are greater than the cohesive forces within the fluid alone. Energy transfer from the fluid to disc occurs by means of momentum diffusion: the momentum of the faster moving fluid layers decreases due to the absorption of particles from slower moving layers. The reverse process contributes to increasing momentum of slower layers.

The most important part, which distinguishes the Tesla turbine from others, is the rotor. It consist of multiple thin disc mounted on a common shaft. Between the discs, spacers are placed whose aim is to hold the discs at a constant distance from each other during exploitation. Important part of construction is also the supply system. The working medium expands in the inlet nozzle, increasing its speed at the expense of pressure drop. Depending on nozzle geometry, the fluid velocity might be equal to or even greater than the speed of sound [9]. Working medium flows tangentially to the discs' surfaces, where the expansion is continued. Due to high velocity gradients, shear stresses occur and torque is produced, which propels the

rotor. Streamlines from the inlet to the outlet are spirally shaped, due to centrifugal force. The geometry of the outlet system is also very important as it influences parameter distribution in the rotor, power output and shape of outlet flow.

The most important issue with Tesla turbine is efficiency. Although rotor efficiency could be very high, as in conventional rotors [10], it is very difficult to design efficient inlet and outlet systems. Neckel and Godinho [9] investigated phenomena occurring in nozzles with the use of Schlieren technique. The most undesirable phenomena which decrease nozzle efficiency was shock wave. They tried to determine geometry, which could decrease total pressure losses and thereby improve overall Tesla turbine efficiency. Hoya and Guha [3] used loss of total pressure as an assessment of nozzle efficiency. Loss coefficient, which express energy degraded by friction, was approximately 10 times higher in nozzle of Tesla turbine than typical value of this coefficient in gas turbine nozzle. Guha and Smiley [11] designed and tested nozzle utilizing a plenum chamber inlet. Experiments showed less than 1 per cent loss in total pressure compared to losses in the range 13-34 per cent for the original nozzle and inlet. Thickness of the gap between the discs also has a great impact on turbine efficiency [12].

Geometry of outlet system also contributes to turbine efficiency loss [13], but there is relatively little literature devoted to that problem. Li et al. [14] conducted experimental study of the Tesla turbine propelled by incompressible fluid. They discovered that rotational speed has a significant influence on exit partial loss.

In this paper, an analysis of the influence of outlet system geometry on parameter distribution and on forming of flow phenomena was carried out. Numerical analysis was performed with the aid of Ansys products: DesignModeler for creating the geometry of the model, Meshing for discretization and CFX 17.0 for physical model and computations.

### Numerical models

Geometry models were based on existing turbine dimensions. The rotor consisted of 5 flat discs of 73 mm diameter, 1,3 mm thickness and 1,5 mm spacing. The rotor of turbine with labels and front view of a single disc are presented in Fig. 1. Flow from the rotor to the outlet system was carried out through 5 holes with diameter of 7,5 mm. Numerical models included only half of the turbine, i.e. two discs and one surface of the third disc, supply and outlet systems (labelled in Fig. 1a as computational domain). Detailed models of computational domains with labels are shown in Fig.2.

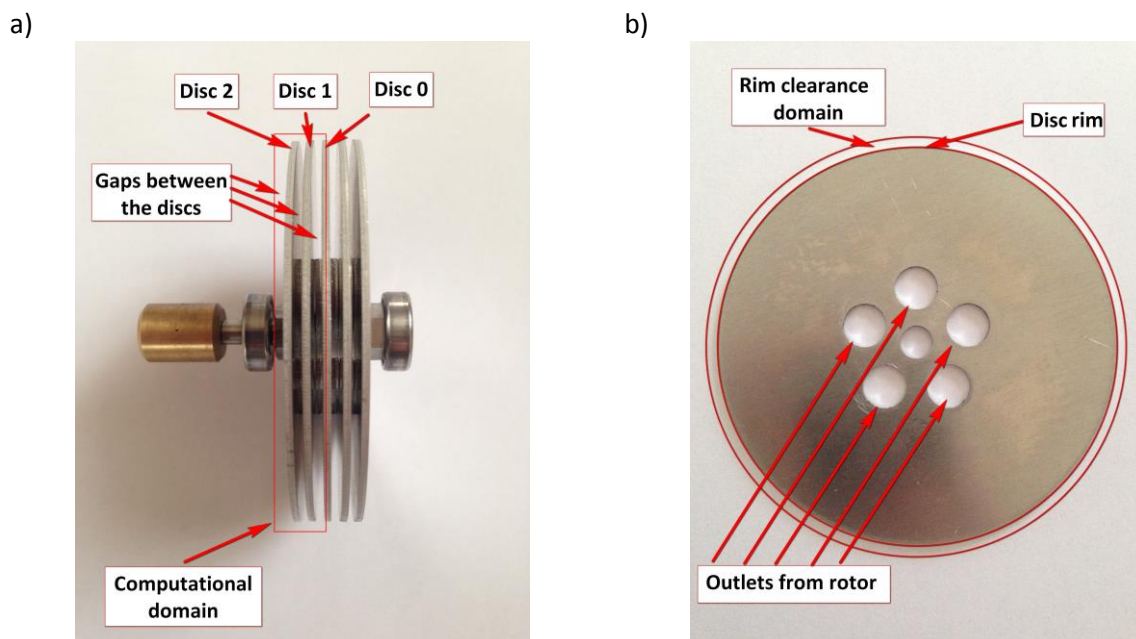


Fig. 1 a) Rotor of the Tesla turbine with labels and b) front view of single disc

Source: Author's

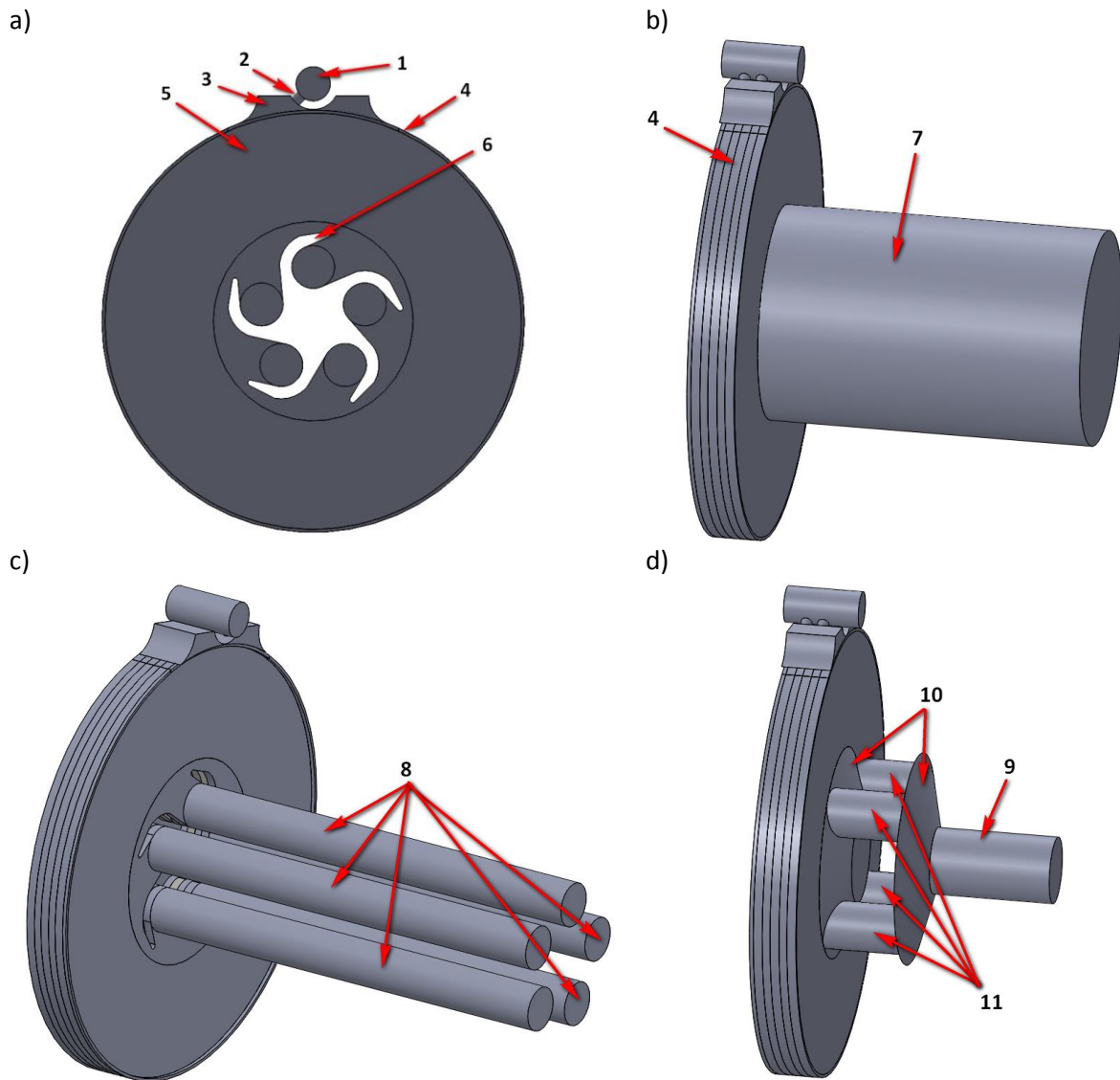


Fig. 2. Computational domains: a) front view of models with spacers, b) model I, c) model II, d) model III  
Source: Author's

The supply system consisted of a supply chamber (label 1 in Fig. 1a), from which the medium was delivered between the rotor discs by means of two holes in the chamber wall (2). Domain labelled 3 represents space between inlet system and rotor. The rim clearance (4) between the discs rims and turbine casing was also modelled. The gap between the discs in which outflow from inlet ducts was carried out, is labelled as number 5. Only in case of disc 1 propulsion was carried out in both sides of the disc. In models II and III the impact of spacers (one of them is labelled 6), which are placed between the discs was taken into consideration. Spacers were responsible for holding constant distance between the discs during operation but also contributed to outflow organization due to their characteristic shape. In model I the outlet system was placed instead of shaped spacers. It consisted of one cylinder (7) with a diameter of 35 mm. In model II the spacers were taken into consideration. Outflow was carried out by means of five cylinders (8) with diameter of 7,5 mm. Model III reflected the exact outlet system geometry of existing turbine, consisting of an outflow duct (9) to ambient air and two choking chambers (10) connected to each other by 4 cylindrical linkages (11). In this model, spacers were also taken into consideration.

In order to obtain results which are unaffected by the discretization method applied to the gap between the discs and inlet system, a mesh independence study was performed. To do so, computations on five different unstructured meshes were carried out and the values of power output were compared. Power obtained from

the finest mesh was considered as reference power, to which other result were compared. In Fig. 3 part of the mesh no. 3 is depicted.

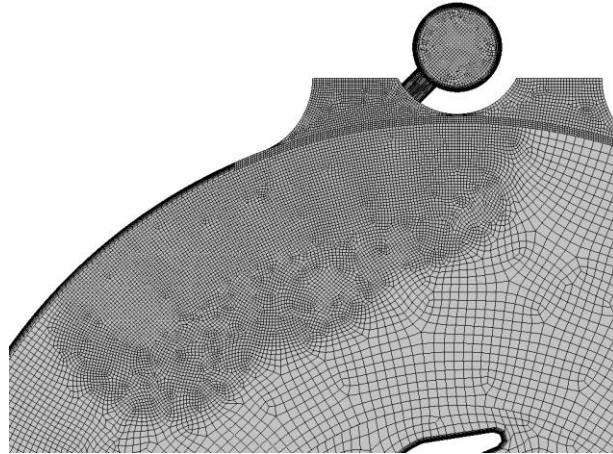


Fig. 3 Part of model discretization  
Source: Author's

Mesheres were finer in areas with a high velocity gradient, i.e. after inlet ducts where the jet was being formed. Furthermore, due to phenomena occurring in boundary layer, which are extremely important in shear stress generation, discretization of this area had to provide distribution of  $y^+$  parameter below 1 throughout the whole domain between the discs. The same method of discretisation was utilised for the inlet system in order to obtain an appropriate model of flow contraction at the inlet duct.

Computations were performed in a steady state, single precision solver. Equations of mass, momentum and energy conservation were solved [15]:

$$\frac{\partial \rho}{\partial t} + \nabla \cdot (\rho \mathbf{U}) = 0 \quad (1)$$

$$\frac{\partial \rho \mathbf{U}}{\partial t} + \nabla \cdot (\rho \mathbf{U} \otimes \mathbf{U}) = -\nabla p + \nabla \tau \quad (2)$$

$$\frac{\partial \rho h_{tot}}{\partial t} - \frac{\partial p}{\partial t} + \nabla \cdot (\rho \mathbf{U} h_{tot}) = \nabla \cdot (\lambda \nabla T) + \nabla \cdot (\mathbf{U} \cdot \tau) \quad (3)$$

The stress tensor  $\tau$  is related to the strain rate by means of the following expression:

$$\tau = (\mu + \mu_t) \left( \nabla \mathbf{U} + (\nabla \mathbf{U})^T - \frac{2}{3} \delta \nabla \cdot \mathbf{U} \right) \quad (4)$$

Working medium was air treated as an ideal gas with constant dynamic viscosity and thermal conductivity. Parameters at the inlet were: absolute total pressure 3 bar and total temperature 303 K. Domains of gap between the discs were stationary, although walls of these domains were rotating with velocity equal to 21000 rev/min. It simulated rotational movement of disc, because walls of the disc are also walls of gap between the discs domain. In addition no slip wall boundary condition was set on these walls. In case of models II and III, spacer domains were also rotating with the same velocity as disc walls. This domains were connected with domains of gap between the discs with frozen rotor interface. In models I and III outlet systems were stationary, but in model II five cylinders were rotating with the same angular velocity as the spacers. It is caused by a fact, that these cylinders are jointed directly with spacer domain. An opening boundary condition with pressure of 1 bar and temperature of 293 K was implemented at the outlet in models I and II. In model III, an outlet boundary condition with average static pressure 1 bar was applied. All flow parameters were based on results obtained from experimental data. High resolution advection scheme and high resolution turbulence numerical scheme were utilised. Conservative auto timescale control with 0.5 timescale factor was applied. The convergence criterion for residuals was set as  $10^{-3}$ .

It was important to obtain as accurate solution for the boundary layer as possible due to a fact that shear stresses, which determine power, are generated in that region. This condition could have been satisfied by using  $k-\omega$  turbulence model. On the other hand, this turbulence model does not provide accurate results for the freestream region, which could lead to wrong conclusions regarding phenomena developing e.g. in the jet. Rotation also introduced effects on turbulence like inverse flow or inhomogeneities, which were additional difficulties in modelling. Large Eddy Simulations are confirmed to provide appropriate level of modelling for rotating flows with fully turbulent regimes [16]. However computational cost is significantly higher compared to RANS simulations. Therefore  $k-\omega$  SST model was employed, which is also often and successfully used in modelling of the Tesla turbine, e.g. in [17].

## Results

In the Fig. 4 dependence of the number of mesh elements on the power is depicted. It can be seen, that the mesh with 4 100 000 elements (4 263 000 nodes) provides sufficient level of accuracy. The boundary layer mesh providing distribution of  $y^+$  below 1 consisted of 24 layers with the first element of  $5 \cdot 10^{-5}$  m of height. Results of computation performed with use of this discretisation method are presented below.

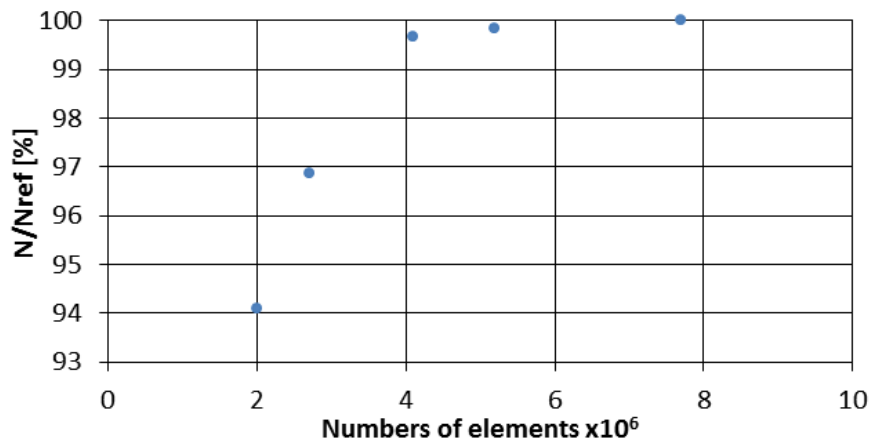


Fig.4. Dependence of the number of mesh elements on the power  
Source: Author's

Power obtained from preliminary experiment and model III are compared to each other. Value computed in numerical analysis has to be multiplied by two, because only half of the turbine was modelled. Results are presented in Tab. 1.

Tab. 1 Comparison of the power obtained from the numerical analysis and the experiment

Experimental analysis (W)	Numerical analysis (W)	Relative difference (%)
41,6	54,2	23,2

Source: Author's

The relative difference is equal to 23,2 %. Taking into consideration fact, that this is only preliminary experiment, convergence of the results might be considered as satisfying. As far as numerical analysis is concerned, simulation did not take into account nonstationary effects, which possibly could change value of power. Therefore computations in unsteady state might provide better results. Additionally application of Large Eddy Simulations as turbulence model could also improve prediction of turbine performance.

In the Fig. 5 static pressure distribution in the middle of gap between the discs 0 - 1 and a comparison between models II and III are presented. It can be observed that the working medium in each model expands in inlet duct to pressure of approximately 120 kPa. This pressure is smaller than the critical pressure for the given conditions (158 kPa) so the Mach number is greater than 1. Mach number distribution is shown in Fig. 6.

The pressure at the outlet from the inlet duct is too high for the conditions in the gap between the discs; hence, overexpansion and overcompression occur. These phenomena take place alternately and slowly diminish. The working medium forms a jet which spreads from the inlet of the duct to the rims of the discs. The maximum Mach number in the jet is observed slightly after the inlet and is equal to 1,3. The jet is bent towards the disc rims due to centrifugal forces acting on the fluid particles. These forces come from the high rotational velocity. Between the jet and disc rims “swirled region” occurs, i.e. an area with a low velocity and unorganized flow. This is a disadvantageous phenomenon, as this area, located far from the axis of the turbine shaft, powered properly could significantly increase the generated torque and power of the turbine. Furthermore, the current supply system configuration causes swirls and backflows, which also decrease torque. The parameter distributions depicted in this area differ depending on the model. In model I “swirled region” has the greatest area its velocity fluctuates between  $5 \text{ ms}^{-1} - 70 \text{ ms}^{-1}$ . In model II this region has the smallest area and a velocity between  $50 \text{ ms}^{-1} - 90 \text{ ms}^{-1}$ . In model III the velocity is between  $5 \text{ ms}^{-1} - 55 \text{ ms}^{-1}$  and the area of this region smaller than in model I and greater than in model II. Another undesirable phenomenon is leakage in the rim clearance. Medium expands beyond the limits of the rotor and thus does not contribute to generation of torque. Differences in Mach number and static pressure distribution between models II and III are shown in Fig.5d and Fig.6d. It can be observed that the biggest differences are in the jet area (up to 0,5 Mach and 7 kPa) and in the outlet system. The jet direction is also different, caused by, among others, different outlet system geometries.

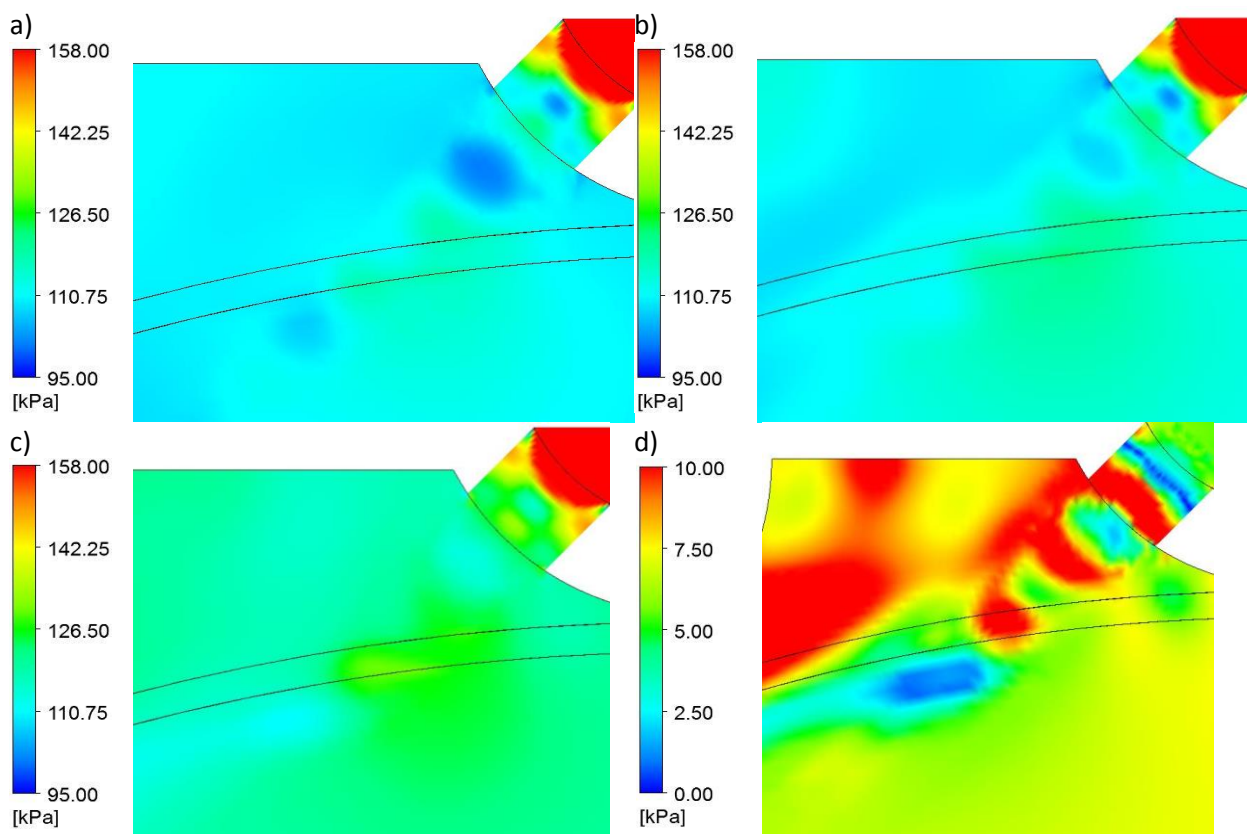


Fig. 5 Static pressure distribution a) in model I, b) in model II, c) in model III and d) difference between models II and III

Source: Author's



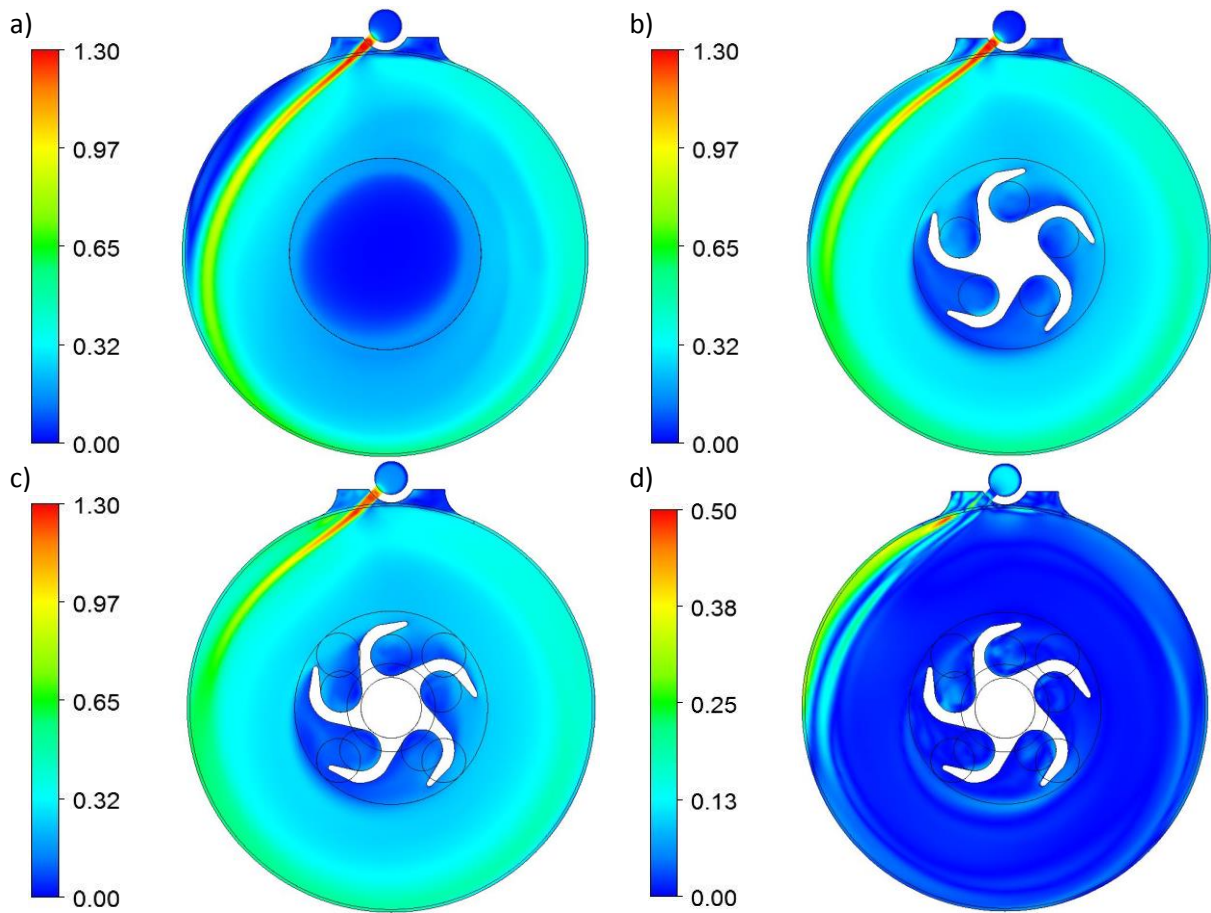
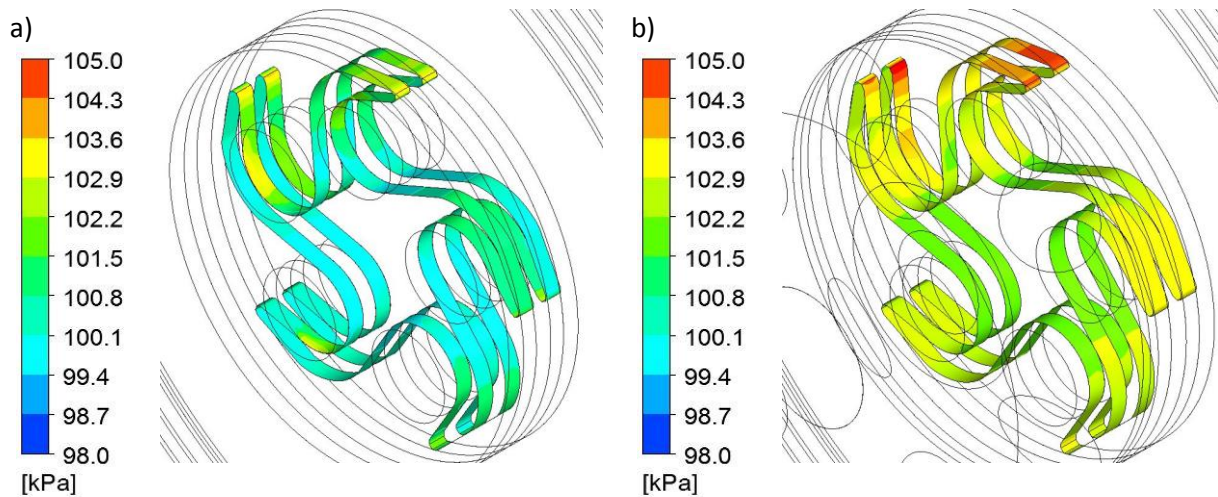


Fig. 6 Mach number distribution a) in model I, b) in model II, c) in model III and d) difference between models II and III  
 Source: Author's

The geometry of model III is more complicated which causes a larger pressure drop in the outlet system; hence, expansion between the discs is carried out to a greater extent than in model II. This can be observed in Fig. 7, which presents the static pressure distribution on the spacer walls.



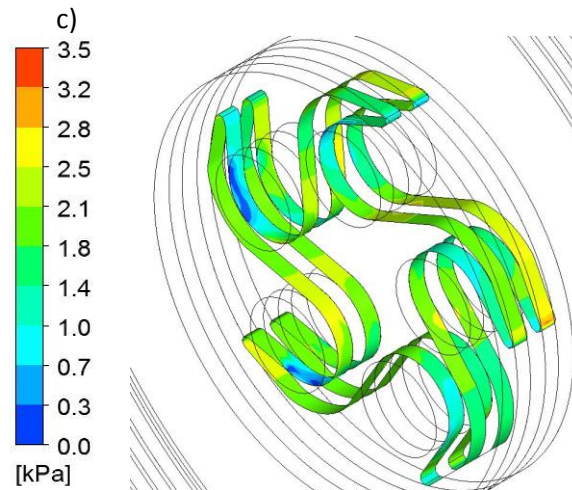
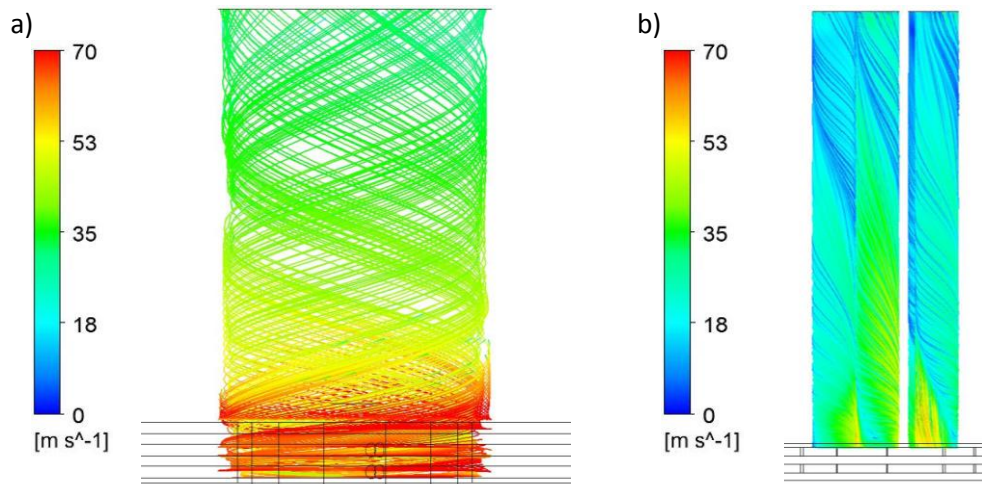


Fig. 7 Static pressure on spacers a) in model II b) in model III c) difference between models II and III  
Source: Author's

The maximum value of static pressure acting on the spacers in model III is equal to 105 kPa and minimum is equal to 99 kPa. In model II, the average static pressure is lower than in model III, with a difference of up to 3,5 kPa. The pressure force acts on the walls of the spacers, so additional torque is generated in this area.

In Fig. 8 streamlines in the outlet systems are presented. In each model, the outlet jet is strongly swirled. In the middle of the swirls, negative pressure (approximately 2 kPa) occurs. This could lead to small backflows into elements of outlet system. The average outflow velocities in models I, II and III are equal to:  $15,15 \text{ ms}^{-1}$ ;  $25,92 \text{ ms}^{-1}$  and  $34,45 \text{ ms}^{-1}$  respectively. This velocity depends on the diameter of the outlet duct, so in model I, where the diameter of the outlet section is largest, the velocity is relatively small. Higher velocities in the outlet section leads to greater kinematic loss. In model III presence of 2 choking chambers did not prevent flow from forming swirled structures.





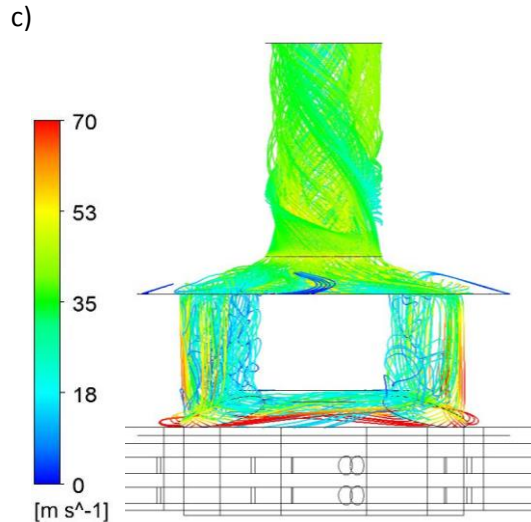


Fig. 8 Streamline in outlet system of a) model I, b) model II, c) model III  
Source: Author's

For each model, the power output based on torque and angular velocity was obtained. Torque was computed from shear stress and distance from the shaft axis. Shear stress values were calculated based on velocity gradient, dynamic viscosity and eddy viscosity. Power was calculated for disc surfaces, disc rims and spacer walls. The results are presented in Tab. 2.

Tab.2 Power obtained from numerical models

Area	Power [W]		
	Model I	Model II	Model III
Disc 1	10,68	13,04	11,36
Disc 2	7,10	8,06	7,83
Disc 0	5,27	6,93	6,07
Rim 1	0,69	0,86	0,67
Rim 2	0,71	0,67	0,69
Rim 0	0,06	0,02	-0,04
Spacer 1	-	0,99	0,33
Spacer 2	-	1,17	0,19
<b>Total</b>	<b>24,51</b>	<b>31,74</b>	<b>27,10</b>

Source: Author's

The highest power was obtained from model II. The differences between the models in power generated by the discs are partially caused by the "swirled region". In model II, this region was the smallest with a relatively high velocity so additional torque was produced. The opposite situation occurred in model I which had the largest area of "swirled region" and a resulting lower power than model II. Differences in the power generated by each discs can be explained by the method of working medium delivery. Disc 1 was propelled from both sides, whereas discs 0 and 2 were only propelled from one side. The rims of the discs also contributed to power generation, but to a lesser extent (0,69 – 0,86 W). In model II, the impact of spacers is greater than in model III. Higher pressure acting on the spacer walls does not contribute to higher power.

### Conclusions

The aim of the investigation presented in this paper was a numerical analysis of the outlet system geometry and its influence on flow phenomena occurring in a Tesla turbine. Geometry model was based on the

dimensions of existing turbine. Three different outlet system were investigated. A mesh independence study was performed and computations were carried out for air, treated as an ideal gas, at inflow conditions of total pressure 3 bar, total temperature 303 K and rotational velocity 21000 rev/min. It was observed that working medium achieved Mach number  $M = 1,3$ . Overexpansion and overcompression occurred after the inlet duct, which, due to its non-isentropic nature, caused a decrease in generated power. In the “swirled region” which occurred between the jet and disc rims, backflows and swirls were present. Elimination of this area could contribute to an increase in the generated power. It was observed that in the rotor in model III, the pressure drop was slightly lower than in the other models. Spacer walls did not contribute significantly to power generation, but did help to organize outflow. The highest power was in case of model II and it was 17,1% higher value compared to the model of existing turbine, which indicates that there is a room for improvement. The power obtained from model III was in a relatively good agreement with the experimental data.

The outlet system is essential for optimal performance in Tesla turbine; hence, its shape should be optimised with respect to flow parameters and rotor geometry.

### Acknowledgement

This research was supported in part by PLGrid Infrastructure. The presented work was supported by the Silesian University of Technology within statutory research funds.

### References

- [1] N. Tesla, Turbine, Patent no: 1,061,206., United States Patent Office of New York N. Y. 1913
- [2] E. Lemma, R.T. Deam, D. Toncich, R. Collins, Characterisation of a small viscous flow turbine, *Experimental Thermal and Fluid Science* 33 (2008) 96-105
- [3] G.P. Hoya, A. Guha, The design of a test rig and study of the performance and efficiency of a Tesla disc turbine, *J. Power and Energy* 223 (2009) 451-465
- [4] S. Sengupta, A. Guha, A Theory of Tesla disc turbines, *Journal of Power and Energy* 226(2012) 650-663
- [5] P. Lampart, Ł. Jędrzejewski, Investigations of aerodynamics of Tesla bladeless turbine, *Journal of Theoretical and Applied Mechanics* 49 (2011) 477-499
- [6] B.P. Ho-Yan, Tesla turbine for pico hydro applications, *Guelph Engineering Journal* 4 (2011) 1-8
- [7] V.P. Carey, Assessment of Tesla turbine performance for small scale Rankine combined heat and power systems, *Journal of Engineering for Gas Turbines and Power* 132 (2010) 122301-1 – 122301-8
- [8] S. Sengupta, A.Guha, Flow of a nanofluid in the microspacing within co-rotating discs of a Tesla turbine, *Applied Mathematical Modelling* 40 (2016), 485-499
- [9] A.L. Neckel, M. Godinho, Influence of geometry on the efficiency of convergent – divergent nozzles applied to Tesla turbines, *Experimental Thermal and Fluid Science* 62 (2015) 131-140
- [10] H. Gupta, S.P. Kodali, Design an operation of Tesla turbo machine – a state of the art review, *International Journal of Advanced Transport Phenomena* 02 (2013) 7-14
- [11] A.Guha, B. Smiley, Experiment and analysis for an improved design of the inlet and nozzle in Tesla disc turbines, *Proceedings IMechE, Part A: J Power and Energy* 224 (2010), 261-277
- [12] R. Puzyrewski, K. Tesch, 1D model calibration based on 3D calculations for Tesla turbine, *Task Quarterly* 14 (2011) 237-248
- [13] W. Rice, Tesla turbomachinery, *Proceedings of IV International Nikola Tesla Symposium* (1991)
- [14] R. Li, H. Wang, E. Yao, M. Li, W. Nan, Experimental study on bladeless turbine using incompressible working medium, *Advances in Mechanical Engineering* 9 (2017), 1-12
- [15] Ansys 17.0 documentation (2016)
- [16] S.Harmand, J. Pellé, S.Poncet, I.V. Shevchuk, Review of fluid flow and convective heat transfer within rotating disk cavities with impinging jet, *International Journal of Thermal Science* 67 (2013), 1-30
- [17] P. Lampart, K. Kosowski, M. Piwowarski, Ł. Jędrzejewski, Design analysis of Tesla micro-turbine operating on a low-boiling medium, *Polish Maritime Research* 63 (2009) 28-33